Dynamical charge density waves rule the phase diagram of cuprates

S. Caprara,[1,2] C. Di Castro,[1,2] G. Seibold,[3] and M. Grilli[1,2]

[1]*Dipartimento di Fisica, Università di Roma "La Sapienza," P.[le] Aldo Moro 5, 00185 Roma, Italy*
[2]*ISC-CNR and Consorzio Nazionale Interuniversitario per le Scienze Fisiche della Materia, Unità di Roma "Sapienza"*
[3]*Institut für Physik, BTU Cottbus-Senftenberg - PBox 101344, D-03013 Cottbus, Germany*

In the last few years, charge density waves (CDWs) have been ubiquitously observed in high-temperature superconducting cuprates and are now the most investigated among the competing orders in the still hot debate on these systems. A wealth of new experimental data raises several fundamental issues that challenge the various theoretical proposals. We here relate our mean-field instability line T_{CDW}^0 of a strongly correlated Fermi liquid to the pseudogap $T^*(p)$ line, marking in this way the onset of CDW-fluctuations. These fluctuations reduce strongly the mean-field critical line. Controlling this reduction via an infrared frequency cutoff related to the characteristic time of the probes, we account for the complex experimental temperature versus doping phase diagram. We provide a coherent scenario explaining why different CDW onset curves are observed by different experimental probes and seem to extrapolate at zero temperature into seemingly different quantum critical points (QCPs) in the intermediate and overdoped region. The nearly singular anisotropic scattering mediated by these fluctuations also accounts for the rapid changes of the Hall number seen in experiments and provides the first necessary step for a possible Fermi surface reconstruction fully establishing at lower doping. Finally, we show that phase fluctuations of the CDWs, which are enhanced in the presence of strong correlations near the Mott insulating phase, naturally account for the disappearance of the CDWs at low doping with yet another QCP as seen by the experiments.

I. INTRODUCTION

The phase diagram of high-temperature superconducting cuprates (HTSC) is quite rich and indicates the coexistence of and the competition between different physical mechanisms. First of all, strong electron-electron correlations give rise to an antiferromagnetic (AF) Mott insulating phase when the CuO_2 planes are half-filled (one hole per unit cell). Although the AF phase is rapidly disrupted by doping, nearly critical spin fluctuations extend their action in the metallic phase. A major distinctive feature is then a pseudogap phase occurring below the doping-dependent temperature $T^*(p)$ [in the prototypical HTSC family YBa$_2$Cu$_3$O$_y$ (YBCO) $T^* \sim 220$–250 K at doping $p \sim 0.1$–0.12 and rapidly decreases merging with the SC T_c around optimal doping and seems to vanish at doping $p^* \approx 0.19$]. The pseudogap phase is characterized by the occurrence of many anomalies like the formation of Fermi arcs extending from the nodal region and the suppression of quasiparticle states around the M points of the Fermi surface, the suppression of the paramagnetic spin susceptibility and the detection of charge density wave (CDW) fluctuations by the fast x-ray probe [1–4], which transform into long-range ordered phase as also detected by the slow probe NMR [5,6], when superconductivity is suppressed by high magnetic fields. An intense debate is ongoing about the sources of this pseudogap phase with essentially two opposite points of view. Since the early times the idea was put forward (mostly by P. W. Anderson [7]) that these systems are strongly correlated doped Mott insulators, where the large electron-electron repulsion and the consequent short-range AF correlations, inside the low dimensional layered structure of the cuprates render these systems intrinsically different from standard metals ruled by the Landau Fermi liquid (FL) paradigm. In this framework, many variants have been proposed ranging from the Luttinger liquid

and the resonating-valence-bond paradigms [7] and its gauge-field relatives [8], to the doped d-wave Mott state [9] to the fractionalized Fermi liquid [10]. The occurrence of this non-FL phase may imply a drastic rearrangement of the fermionic states: while far from the Mott state a FL is present with a large Fermi surface containing $n_h = 1 + p$ holes per unit cell in the CuO_2 planes, approaching the Mott state the metallic character is given by just p carriers residing in four hole pockets in the so-called nodal regions $(\pi/2a)(\pm 1, \pm 1)$ of the Brillouin zone [8–10]. According to Ref. [10], T^* marks a topological transition related to this change of Fermi surface dimensions.

The other point of view is that in two dimensions, strong correlations and the short-range AF correlations of a doped Mott insulator are not enough *per se* to spoil the Landau FL [11] and to establish the onset at high doping of the anomalous behavior of the metallic cuprates. This, instead, should be marked by the proximity to some form of instability ending at zero temperature into a second-order transition (quantum critical point, QCP). In this case the incipient order, which at low or zero temperature has an intrinsic quantum (and therefore dynamic) character produces strong long-ranged and long-lived fluctuations. In turn, these mixed quantum-thermal fluctuations mediate strong scattering between the quasiparticles spoiling the FL character of (some of) the quasiparticles, possibly mediating a strong superconducting pairing. In this "quantum criticality" scenario a crucial role is obviously played by the type of order that the system would like to realize. Although many proposals have been put forward, the old evidences of charge density waves (CDW) [12–14] have been strongly revived by the recent ubiquitous observations of charge density waves (CDWs) in all HTSC families.

The observed CDWs (see, e.g., Refs. [1–6,15–22]) appear as a long-ranged phase under special circumstances only, like when high magnetic fields suppress superconductivity
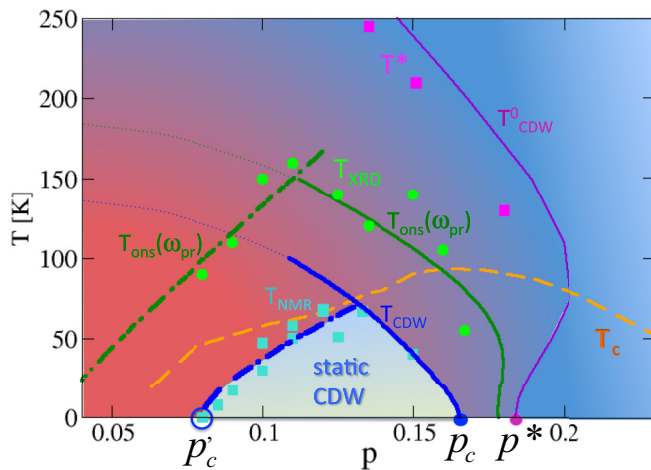
FIG. 1. Summary YBCO phase diagram. Increasing reddish hue corresponds to more well-defined CDW amplitude correlations. Experimental curves: orange dashed line: superconducting critical temperature $T_c(p)$; magenta squares: pseudogap crossover line (from Ref. [23], but see also Fig. 6 of Ref. [24]); green circles: CDW onset temperature from x-ray scattering experiments [4,22]; light blue squares: static CDW order as obtained from NMR [5,6], which coincides with the onset of the FS reconstruction as detected by R_H measurements [18]. On the optimal/overdoped side the magenta solid line tracks the mean-field CDW transition temperature identifying the region below which CDW fluctuations (of both modulus and phase) become prominent. The blue solid line is the static CDW transition line taking quantum/thermal fluctuations beyond mean-field into account. The intermediate green solid curve reports the dynamical CDW onset for probes having characteristic frequency $\omega_{pr} = 50$ K (see text). On the underdoped side, the blue dot-dashed line represents the CDW transition ruled by phase fluctuations of the CDW order parameter (see text). In the region below, the blue solid line (and of the thin dotted line as a guide to the eye) and above the blue dot-dashed line the modulus of the CDW order parameter is finite, while phase fluctuations destroy the static order (possibly leaving a vestigial nematic order). The thick green dot-dashed line marks the dynamical onset observed by dynamical probes. This line is similar to the green solid line, but only phase fluctuations are involved here. The magenta dot marks the endpoint of the pseudogap crossover line at $p^* \approx 0.19$, identified with the endpoint of the mean-field transition, $p^* = p_c^0$. The solid blue dot is the true CDW-QCP at $p_c \approx 0.16$ (with fluctuations taken into account), while the blue circle at $p_c' \approx 0.08$ is the low-doping QCP where the CDW phase stiffness vanishes.

[5,6,15]. Figure 1 reports the phase diagram of YBCO, where the light-blue squares mark the onset of this static CDW order as detected by NMR [5,6], over a doping range where Hall experiments (see Ref. [18] and references therein) detect a Fermi surface reconstruction, which is there attributed to CDW order. Dynamical onset of CDWs, theoretically predicted long ago [12,13,25,26], has been observed via x-ray spectroscopies [1–4,22] (green circles in Fig. 1). Recent Hall effect measurements indicate that a Fermi-surface reconstruction takes place in YBCO [18] and La$_{2-x}$Sr$_x$CuO$_4$ (LSCO) [27] at low temperature starting at doping $p_c' \approx 0.08$ and ending into a QCP at $p_c \approx 0.16$. On the other hand, the number of carriers changes rapidly between $p_c \approx 0.16$ and $p^* \approx 0.19$, where $T^*(p)$ extrapolates to zero, with a clear connection to the

above "Mottness" versus "quantum-criticality" issue discussed above. p_c and p^* are distinct and from the "Mottness" point of view one may argue that, while p^* marks the physical onset of a novel non-FL metallic phase, p_c is the start of the CDW phase, which is a mere "epiphenomenon" occurring "on top" of the more fundamental non-FL state. Conversely, as supporters of the second point of view, we stress the close proximity of p_c and p^* claiming that CDW play the central role with their QCP at $p_c = 0.16$, while p^* is a crossover doping marking the region where, among other characteristic properties of the pseudogap, the strong CDW fluctuations appear before the QCP is met.

We exploit the recent experimental data to shape a coherent scenario based on the "quantum critical" point of view, which rationalizes the following issues: (a) how the different CDW onset curves and corresponding seemingly different QCPs are related to one another? (b) Are the CDWs related or unrelated to the pseudogap onset temperature $T^*(p)$? (c) Can CDWs account for the rapid changes of the Hall number seen in experiments? (d) Which is the mechanism leading to the disappearance of the CDWs at low doping with yet another QCP located at $p_c' \approx 0.08$, as detected for YBCO in Ref. [18]? We concentrate our analysis on YBCO, for which the most complete set of experiments has been collected. Our results in comparison with experiments are summarized in the phase diagram of Fig. 1 and can be directly extended to Bi$_2$Sr$_2$CaCu$_2$O$_{8+x}$ (Bi2212) (see, e.g., Refs. [3,20]), and Bi$_2$Sr$_{2-x}$La$_x$CuO$_{6+\delta}$, Bi$_2$Sr$_{2-x}$La$_x$CuO$_{6+\delta}$ (Bi2201). As far as LSCO is concerned, due to the strong similarity of behavior with YBCO in the optimal and high doping regime, all the results connected with the strongly correlated Fermi liquid instability are valid. At low doping a particular care has to be taken due to the strict relation between the spin and charge modulation vectors [28,29].

Our paper is organized as follows: Sec. II initially revisits the frustrated phase separation mechanism underlying the formation of incommensurate CDW in strongly correlated systems. From this starting point, a new analysis is carried out explaining why the strong correlations of HTSC favor the occurrence of CDW along the observed directions of the Cu-O bonds. The dynamical character of the CDW fluctuations is then analyzed to explain why probes with different characteristic time scales may detect different CDW onset temperatures. Section III provides a possible explanation for the rapid change in carrier density observed by Hall experiments based on the strongly anisotropic scattering induced by CDW fluctuations. In Sec. IV, again starting form the strongly correlated character of cuprates, we propose a mechanism to explain why CDW tend to weaken and disappear in the low-doping region of the phase diagram. In Sec. V, we discuss our findings and we present our concluding remarks.

II. THE OPTIMAL/OVERDOPED PHASE DIAGRAM: DYNAMICAL CDW CROSSOVERS AND CDW TRANSITION

Before addressing the above (a)–(d) issues, we revisit the frustrated phase separation mechanism, which was proposed long ago [30,31] as the formation mechanism of CDW, giving rise to a QCP around optimal doping [25]. The region around
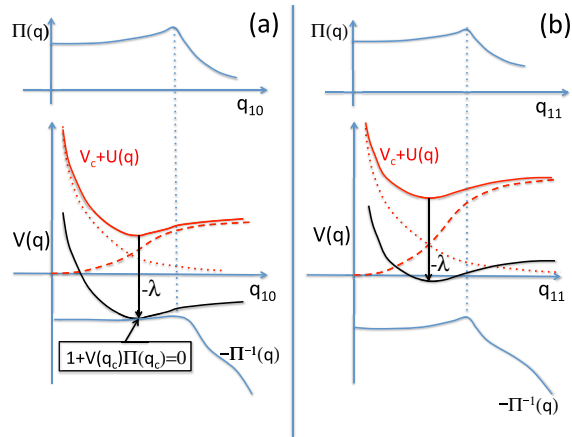
FIG. 2. Sketch of the *ingredients* determining the CDW instability and its wave vector. (a) Upper panel: Lindhard polarization function $\Pi(\mathbf{q})$ with $\mathbf{q}$ along the $(1,0)$ or $(0,1)$ directions. Lower panel, black solid line: residual interaction $V(\mathbf{q})$ among quasiparticles, arising from the sum of the Coulomb repulsion (red dotted line), the short-range residual repulsion $U(\mathbf{q})$ (red dashed line), and a nearly momentum independent attraction λ shifting downwards the repulsive interaction. The instability occurs when $V(\mathbf{q}_c) = -\Pi^{-1}(\mathbf{q}_c)$. (b) Same as (a), but in the $(1,\pm 1)$ directions, where $U(\mathbf{q})$ is stronger and the same λ is not enough to render the system unstable: $V(\mathbf{q}) > -\Pi^{-1}(\mathbf{q})$ for all $\mathbf{q}$'s.

optimal doping is naturally described within a Fermi-liquid picture and CDWs occur as a second-order instability. The correlated character of the Fermi liquid is described within a standard Slave-boson/Gutzwiller approach, where the residual interaction among the quasiparticles $V(\mathbf{q}) = U(\mathbf{q}) - \lambda + V_c(\mathbf{q})$ arises from three distinct contributions (see Appendix A): $U(\mathbf{q})$ is a short-range residual repulsion stemming from the large repulsion of a one-band Hubbard model, λ is a local short-range attraction triggering charge segregation, due to a local phonon [25], to the instantaneous magnetic interaction present in doped antiferromagnets [32], or to both mechanisms, and $V_c(\mathbf{q})$ is the long-range part of the Coulomb repulsion. Notice that even if phonons are involved in λ, they are not directly related with pairing. The screening processes are described by the Lindhard polarization bubble $\Pi(\mathbf{q},\omega_n)$ for quasiparticles having a renormalized band structure fitting the dispersion obtained from angle-resolved photoemission spectroscopy (ARPES) experiments. The CDW instability is found as a divergence of the density-density correlation function, when $1 + V(\mathbf{q})\Pi(\mathbf{q},\omega_n) = 0$ at $\omega_n = 0$ and $\mathbf{q} = \mathbf{q}_c$ [12,25,26]. For its pictorial representation see Fig. 2. In our mechanisms, strong correlations favor the CDW instability along the $(1,0)$ or $(0,1)$ Cu-O bond directions, in agreement with hard x-ray experiments [22]. Indeed, these are the directions along which the short-range repulsion [see Fig. 2(a) and Appendix A] is smaller, making the instability of the frustrated phase separation due to the local effective attraction λ easier. This shows that the frustrated phase separation mechanism naturally exploits the strongly correlated nature of HTSC to account for the occurrence of CDW along the ubiquitously observed $(1,0)$ or $(0,1)$ directions.

Expanding $V(\mathbf{q})$ and $\Pi(\mathbf{q},\omega_n)$ around $\mathbf{q} = \mathbf{q}_c$ and $\omega_n = 0$ one obtains the standard quantum-critical charge-fluctuation propagator (see Appendix A):

$$D(\mathbf{q},\omega_n) = \left[m_0 + \nu(\mathbf{q}) + |\omega_n| + \omega_n^2 / \overline{\Omega} \right]^{-1}, \qquad (1)$$

where $m_0 \propto \xi_0^{-2} \propto 1 + V(\mathbf{q}_c)\Pi(\mathbf{q}_c,0)$ is the mean-field *mass* of the fluctuations, ξ_0 is the mean-field CDW correlation length, $\nu(\mathbf{q}) \approx \bar{\nu}|\mathbf{q} - \mathbf{q}_c|^2$, $\bar{\nu}$ is an electronic energy scale (we work with dimensionless momenta, measured in inverse lattice spacings $1/a$), and $\overline{\Omega}$ is a frequency cutoff. The mean-field instability line $T_{CDW}^0(p)$ (magenta solid line in Fig. 1) is characterized by a vanishing m_0. This is the well-known frustrated-phase-separation instability [30,31] underlying the formation of CDWs near optimal doping [12,25,26]. We notice that, although λ might have a magnetic contribution, the present mechanism of CDW formation, contrary to other proposals [33–36], does not require the proximity to a magnetic QCP. The same CDW-mediated interactions are also active in the Cooper channel, providing a high-temperature d-wave pairing mechanism [37]. Therefore this region of the phase diagram is characterized also by the gradual onset of CDW-mediated pairing fluctuations, with reducing temperature and/or doping.

The microscopic parameters of the model are adjusted to fix the mean-field QCP at $p_c^0 \approx 0.19$, while the temperature dependence of the mean-field instability line $T_{CDW}^0(p)$ arises from the Lindhard function, *without further adjustable parameters*, and tracks the pseudogap onset line $T^*(p)$. In our scheme, below $T_{CDW}^0(p)$, CDW long-range order would occur, were it not for quantum-critical fluctuations especially relevant because of the quasi-bidimensionality of the cuprates. In real systems, where strong fluctuations are present, below this line, CDW fluctuations become increasingly long-ranged and long-lived, and start to suppress the quasiparticle states preferably in the antinodal regions of the Fermi surface (see Ref. [38] and Appendix D). This spread of the quasiparticle spectral weight away from the Fermi surface gives rise to the density of states suppression characterizing the pseudogap onset temperature T^*. This explains the connection of our theoretical mean-field line $T_{CDW}^0(p)$ with $T^*(p)$. Of course there is no intrinsic cutoff to CDW fluctuations, and these may extend at even higher temperatures than $T_{CDW}^0(p)$, but with shorter and shorter range and time scales.

The fluctuation suppression of the mean-field critical line $T_{CDW}^0(p)$ is obtained by the self-consistent evaluation of the correction to the mean-field mass m_0, due to the fluctuator (1) (see Methods, Fig. 5),

$$m = m_0 + uT \sum_n \int_0^\Lambda d\nu \, \frac{N(\nu)}{m + \nu + |\omega_n| + \omega_n^2/\overline{\Omega}}, \qquad (2)$$

where u is the strength of the coupling between CDW fluctuations, $N(\nu)$ is the density of states corresponding to the dispersion law $\nu(\mathbf{q})$ and Λ is an ultraviolet cutoff, corresponding to a momentum cutoff $\bar{q} \sim 1/a$.

One can numerically solve the self-consistent expression (2), finding the conditions for the instability $m = 0$ and the dependence of m on temperature and doping. In a two-dimensional system, as a single CuO$_2$ plane of cuprates, $N(\nu)$ is constant for $\nu \to 0$. This leads to a finite shift of the two-dimensional QCP at $T = 0$, but the correction to

the critical line at finite T is divergent, consistently with the absence of long-range order in two dimensions for a two-component order parameter (as in the incommensurate CDW case). However, cuprates are layered systems and the planes are weakly coupled. This allows for an ordering at finite temperature $T_{CDW}(p)$, which arises in the solution of Eq. (2) for $m = 0$, provided $N(\nu)$ assumes a three-dimensional form $N(\nu) \sim \sqrt{\nu}$ below some energy scale $\nu_\perp$ related to the inter-plane coupling (see Methods). $T_{CDW}(p)$ is so much reduced (see blue solid line in Fig. 1) with respect to the mean-field line $T_{CDW}^0(p)$, that it occurs below the superconducting dome. Superconductivity therefore appears as the stabilizing phase against CDW long-range order. This explains why the experimental data corresponding to long-range CDWs are only detected for magnetic fields large enough to weaken the superconducting phase [15]. These experiments also allow to estimate $\nu_\perp$. Figure 1 displays the $m(T_{CDW}) = 0$ blue line obtained with $\nu_\perp = 10$ K.

We now address the issue (a) of why different probes identify different CDW onset temperatures. The key point is the dynamical character of the CDW fluctuations. A probe with long characteristic time scale (like, e.g., NMR or NQR) will only detect static order, otherwise the fluctuating CDWs average to zero during the probing time. This is why these probes identify a true phase-transition line $m(T_{CDW}, p) = 0$ at high magnetic field (of course, if in real systems pinning intervenes to create locally a static order, this can be detected by local static probes even at larger temperatures and low magnetic fields. This seems to be the case in recent NMR experiments [19]). On the other hand, a fast probe with a short probing time τ_{pr} takes a fast snapshot of the fluctuating system and finds a seemingly higher transition temperature when the CDW order is still dynamical, as long as the CDW characteristic time scale $\tau_{CDW} \propto \xi^2 \propto m^{-1}$ is longer than τ_{pr}, thus acting as an infrared cutoff and diminishing the reduction effect of the fluctuations on the onset temperature. We identify the dynamical onset line as the line where $m \approx \omega_{pr} = \tau_{pr}^{-1}$. The theoretical green solid line in Fig. 1 obtained in this way with a mass $m \approx \omega_{pr} = 50$ K, represents the dynamical onset of CDWs observed with a fast probe, e.g., x-ray spectroscopy [the green circles in Fig. 1, as measured in Refs. [4,22]. Actually, RIXS and REXS experiments are even faster and upon increasing the signal-to-noise ratio we expect that CDW could be revealed at substantially higher temperatures (possibly even higher than T^*). We thus solved the experimental puzzle (a)] with a unified explanation of how different onset lines for CDWs are detected, running from the long-range order to the fast fluctuations.

III. CDW-QCP INTERPRETATION OF HALL TRANSPORT

According to issue (c), recent Hall experiments [18] show a rapid increase of the Hall number in a narrow doping range from $n_H = p$ at $p \lesssim 0.16$ up to $n_H = 1 + p$ for doping larger than the pseudogap zero temperature onset point p^*. Such crossover has been attributed to a large Fermi surface at $p > p^*$ as observed with ARPES and the formation of hole pockets for $p < p^*$ due to either the establishment of a new metallic phase like a d-wave Mott insulator [9,41] or a "topological metal" [42], or some more conventional kind of order as, e.g., a spin spiral [43]. In all these scenarios p^* is *unrelated* to CDWs whose QCP is then placed at the lower doping value p_c.

Here, instead, we keep a minimal framework showing that the crossover behavior of the Hall number can be explained by the increasingly strong fluctuations starting below $T^*(p)$ and approaching the nearby CDW-QCP. In particular, we exploit the strong momentum dependence of the effective quasiparticle interaction mediated by the CDW propagator Eq. (1) which naturally splits the Fermi surface in *hot* and *cold* regions: the quasiparticles in the hot regions ($\phi = 0, \pi/2$) are connected by $\mathbf{q} \sim \mathbf{q}_c$ and interact strongly, while the scattering in the cold regions stays weak. This results in a marked anisotropy of the quasiparticle scattering rate [44]

$$\Gamma(\phi) = \left\{ \Gamma_{max}^{-1} + [\Gamma_0 + \Gamma_\Sigma(\phi)]^{-1} \right\}^{-1}, \quad (3)$$

with

$$\Gamma_\Sigma(\phi) = \text{Im} \frac{2\, T\, \Gamma_2(\phi)}{1 + \sqrt{1 - i \frac{T}{M(\phi)}}}, \quad (4)$$

and $\Gamma_2(\phi) = \Gamma_2[1 + \alpha \cos^2(2\phi)]$. The expression of $\Gamma_\Sigma(\phi)$ is derived from the quasiparticle self-energy near hot spots in models with spin [45] or charge [44] nearly critical fluctuations. Here, $M(\phi) = m(T) + \bar{\nu} \sin^2(2\phi)$ is the energy scale below which the quasiparticles have a Fermi-liquid behavior and is minimal at the hot spots. The anisotropy of $\Gamma(\phi)$ is enhanced by approaching the CDW criticality, where $m(T)$ vanishes. The resulting fits of R_H as a function of temperature are reported in Fig. 3(a), while the related hole densities are reported in Fig. 3(b) by the blue circles, in good agreement with the experimental values (red squares) [18]. Interestingly, we also find a good agreement with the resistivity curves [see Fig. 7 in Methods] in contrast to a similar analysis in Ref. [18]. The inset of Fig. 3(a) also shows that the anisotropic component of scattering strongly increases with approaching $p_c \approx 0.16$ so that the dominating contribution to n_H is coming from the nodal regions.

The anomalous singular scattering is a general consequence of the CDW-QCP and it *must* occur when this is approached, as it has indeed been measured by quantum oscillations in Ref. [46], and corresponds to the region of Fermi surface reconstruction and of anomalous behavior of the Hall number. Hence, coming from high temperatures, our CDW-QCP scenario predicts a significant increase of R_H upon crossing T_{CDW}^0, i.e., according to our identification, the pseudogap temperature, at which, as mentioned above, the same CDW scattering starts to deplete spectral weight from the antinodal Fermi surface states [38] [see also Appendix D]. However, it is important to note that our analysis does not incorporate pairing fluctuations, which have been shown [39,40] to be relevant in a certain temperature window $T_c < T < T_{pair} < T^*$.

In the present context we speculate that, if long-range superconducting order is suppressed by strong magnetic fields, pairing fluctuations extend down to $T = 0$ in contrast to the anisotropic scattering from Eq. (4), which vanishes in this limit (even though the vanishing of $m(T)$ tempers this reduction). Therefore, upon lowering temperature, the increasing contribution of pairing fluctuations will counteract the decrease in the CDW anisotropic quasiparticle scattering and thus eliminate the downturn of the R_H curves in Fig. 3 in the limit $T \to 0$ as is observed in Nd-codoped LSCO [47]
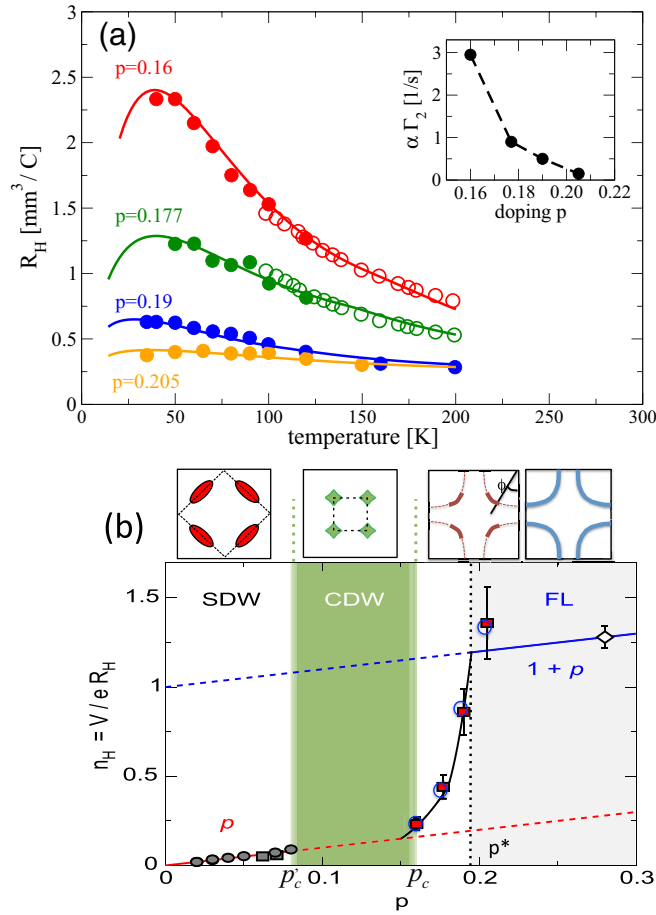
FIG. 3. Analysis of Hall constant and hole density within the CDW-QCP scenario. (a) Fits of R_H vs T of the low-field (empty circles) and high-field (filled circles) measures at various dopings (data taken from Ref. [18]) using the anisotropic scattering model of Eqs. (3) and (4). The anisotropy parameter $\alpha \Gamma_2$ is reported in the inset. (b) (Adapted from Ref. [18]) Doping evolution of the hole density extracted from R_H measurements in Ref. [18]. The experimental points in the range $0.16 \leqslant p \leqslant 0.205$ are the red rectangles with error bars, while the blue circles are the values of n_H extracted from the fits based on the microscopic anisotropic scattering model. The Fermi surfaces in the various doping regimes are schematically depicted above: (from left to right) hole pockets in the strongly correlated region near the Mott transition, Fermi surface reconstruction with electron pockets in the CDW region; large Fermi surface for $p > p_c \approx 0.16$ with dashed (hot) regions where for $T < T_{CDW}^0$ the anisotropic CDW scattering suppresses the quasiparticle states; for $T < T_{pair}$ this suppression is enhanced by CDW-mediated pairing and fluctuations may lead to the formation of Fermi arc features [39,40]; large Fermi surface in the region far from the CDW-QCP, where CDW scattering is weak and the Fermi-surface states are cold.

where R_H can be measured to much lower temperatures than in YBCO where the measures end at $T = 40$ K.

IV. THE UNDERDOPED PHASE DIAGRAM: THE ROLE OF CDW PHASE FLUCTUATIONS

In all the models proposed so far (including ours), were it not for the competing superconducting phase, the critical line for static CDWs monotonically increases with underdoping
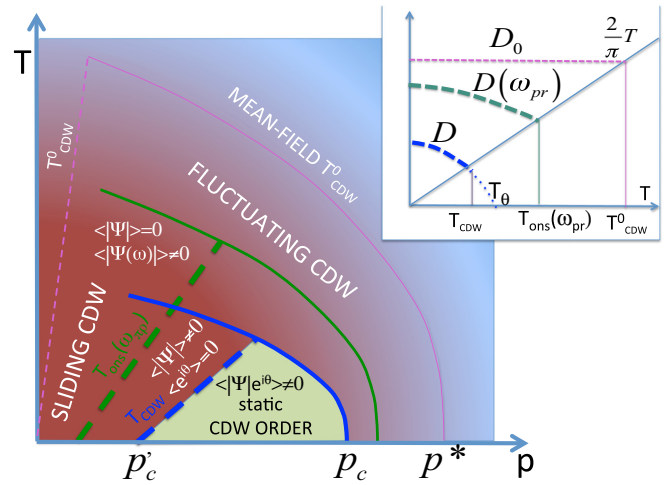
FIG. 4. Schematic view of the phase diagram. The solid magenta line on the right is the mean-field instability line, while the dashed one on the left is the BKT transition temperature as obtained from the *bare* CDW phase stiffness $T_{CDW}^0 = \frac{\pi}{2} D_0$ (see magenta dashed line and thin solid blue line in the inset). The thick solid blue line is the transition line obtained by fluctuations correcting the mean-field instability line. Below this line, the amplitude of the CDW order parameter is finite $\langle |\Psi(0)| \rangle \neq 0$. The analogous line on the left is dashed and arises from the thermal and quantum phase fluctuations reducing the phase stiffness (see blue dashed line in the inset at fixed doping). The intermediate lines arise when fluctuation corrections are cut off in the infrared limit. The green solid line is for amplitude and phase fluctuations, partially reducing T_{CDW}^0. Below this line, the *static* average of the CDW order parameter amplitude vanishes, but it is finite for long time intervals tested by fast probes, $\langle |\Psi(\omega > \omega_{pr})| \rangle \neq 0$: the green dashed line is the onset temperature T_{ons} corresponding to a phase stiffness, which is less reduced because of an infrared cutoff to phase fluctuations (also reported as a green line in the inset for a fixed doping). (Inset) CDW phase stiffness at fixed doping as a function of temperature. The magenta dashed line is the bare stiffness D_0. The blue dashed is the stiffness D corrected by phase fluctuations. Disregarding the discontinuity at the BKT transition, the phase stiffness vanishes at T_θ (dotted blue line). Green dashed line: same as the blue line, but the fluctuations have an infrared momentum cutoff ω_{pr}/c_θ to mimic the stiffness on time scales shorter than ω_{pr}^{-1}.

and saturates to a finite value at low doping (see Figs. 1 and 4 below the solid blue line). This is at odds with the experiments, where CDWs appear below a dome-shaped critical line ending into a QCP at low doping $p_c' = 0.08$ [18,48]. In our model we solve this inconsistency taking into account the role of the dynamical fluctuations of the phase θ of the CDW order parameter $\Psi(\mathbf{r}) = |\Psi(\mathbf{r})|e^{i\theta(\mathbf{r})}$ at low doping.

A well-known feature of CDWs [49] is that their phase stiffness is proportional to the strength of the metallic character (like, e.g., high Fermi velocity, high quasiparticle DOS, etc.), which is strongly reduced in the proximity of the Mott transition. Thus the experimentally observed reduction of the CDW critical (or onset) temperatures in the underdoped region appears as a crossover from a transition ruled by the vanishing of the amplitude of the CDW order parameter $\langle \Psi \rangle = \langle |\Psi(\mathbf{r})| \rangle = 0$ to a transition controlled by the suppression of the stiffness, due to fluctuations of the phase θ. In this region

(below the solid blue line and above the dashed blue line in Fig. 4), the translational symmetry is restored by the sliding motion of the CDW, with the sliding CDW possibly oriented along the a or b direction of the CuO_2 planes, thereby marking a nematic breaking of the C_4 symmetry of the lattice. This situation is reminiscent of the so-called *vestigial* charge order [29,50], obtained in a different context.

The effect of the phase fluctuations on the CDW dynamics is customarily described by the XY-like action

$$\mathcal{S}_{XY} = \frac{1}{8} \sum_{\mathbf{q},\omega_m} \left[D_0 q^2 + \chi \omega_m^2 \right] \theta(\mathbf{q},\omega_m) \theta(-\mathbf{q},\omega_m),$$

where D_0 is the bare stiffness, and the coefficient χ determines the speed $c_\theta = \sqrt{D_0/\chi}$ of the phase fluctuations [49]. As long as the CDW critical temperature is larger than the interplane coupling ($\approx$10 K in the optimal doping region), we can take this transition to be of the Berezinski-Kosterlitz-Thouless (BKT) type. According to the above arguments, the phase stiffness $D_0 \propto p$ and therefore the bare critical temperature of the BKT transition obtained from the usual condition $T_{\mathrm{CDW}}^0 = \frac{\pi}{2} D_0$ (see magenta line in the inset of Fig. 4) is also proportional to doping $T_{\mathrm{CDW}}^0 = \bar{T} p$ (magenta dashed line in Fig. 4).

However, similarly to what happens on the high-doping side to the mean-field critical temperature, whatever is the bare T_{CDW}^0, this is reduced by the quantum and thermal phase fluctuations. Within the XY model with soundlike phase fluctuation modes one obtains the perturbative expression of the depleted stiffness [51]:

$$D = D_0 - \frac{u_\theta\, c_\theta}{2\pi \Lambda_\theta^2} \int_0^{\Lambda_\theta} \mathrm{d}q\; q^2 [1 + b(c_\theta q)], \qquad (5)$$

where $\Lambda_\theta \sim 1/a$ is a momentum cutoff (hereafter we take $\Lambda_\theta = 1$) and $b(z) = [\mathrm{e}^{z/T} - 1]^{-1}$ is the Bose function. Starting from different D_0 at the different doping and calculating the perturbative corrections with a doping-independent coupling u_θ, we reduce the bare BKT transition temperature to $T_{\mathrm{CDW}} = \frac{\pi}{2} D$, which vanishes at a value of $p = p'_c$, thereby answering issue (d) in the Introduction. The various physically relevant combinations of the microscopic parameters can be reduced to two effective parameters only (see Appendix C), the position of the QCP, which can be fixed by experiments at $p'_c \approx 0.08$ and the slope of the $T_{\mathrm{CDW}}(p)$ curve. Numerically solving Eq. (5) we obtain the dashed blue line in Fig. 1.

Above the static T_{CDW} the phase fluctuates dynamically and, similarly to what happens in the high-doping region, a fast probe may detect a seemingly ordered state. This occurs as long as the phase correlation time τ_θ is longer than the characteristic time scale of the probe. Again, we mimic this effect with an infrared cutoff ω_{pr}, i.e., a lower limit $\omega_{\mathrm{pr}}/c_\theta > 0$ in the integral in Eq. (5). The reduced effect of quantum and thermal fluctuations leads to a larger stiffness and, in turn, a CDW onset at a higher temperature. For $\omega_{\mathrm{pr}} = 50$ K, we find the green dot-dashed line in Fig. 1, that matches with the same ω_{pr} the analogous line found in the optimal/overdoped region. The joint onset line then accounts for the dome-shaped $T_{\mathrm{CDW}}(p)$ onset temperature found by x-ray scattering [issue (a) in Introduction].

The prediction of a low-doping CDW-QCP due to the vanishing of the CDW phase stiffness raises the obvious issue of a possible direct observation of the associated strong phase modes in the vicinity of the transition. Since the phasons are optically active [52], optical conductivity is a natural tool to this purpose, but the contribution to the planar optical conductivity from overdamped CDW modes has already been theoretically investigated [53] and it turns out that this contribution is likely overshadowed by the wealth of planar single particle excitations. On the other hand, the optical conductivity along the c-axis $\sigma_c(\omega)$ could be much more suited to identify the effects. In fact, the observed resonance in bilayer (and threelayer) cuprates [54], which has been previously attributed to transverse (Josephson) plasma modes (TPM) [55] might also be associated with intralayer-coupled phason modes which generate a dipole moment along the c direction [56]. The proposed experiment is not a smoking gun experiment, but it would be a valid contribution to test our scenario since the expected specific doping and temperature scaling properties [53] could be a useful test on the origin of this optical feature.

V. DISCUSSION AND CONCLUSIONS

We addressed several key issues of cuprates, and yet other issues remain open. First of all, to be as simple as possible, we considered the single-band Hubbard model. Although attempts have been made to treat (approximately) the intracell charge distribution also in this model [57], this model is not naturally taylored to consider the intracell CuO_2 structure. We thus purposely decided to keep outside the scope of our paper the interesting question of the internal d-wave structure of the CDW order parameter recently detected both in resonant x-ray scattering [58] and STM [21,59] experiments.

We also ignored the effect of disorder, which may locally render the CDW fluctuations static [60] and therefore observable by NMR well above the true static transition line [19]. Nevertheless our scenario is a good starting point to address these remaining open issues since it provides a unified scheme based on a robust and generic frustrated phase-separation mechanism to explain all the (a)–(d) issues listed in the introduction. The direction of the critical CDW wave vector, which is a natural test on the validity of the various proposed CDW mechanisms, is determined here by the generic strong-correlation effect encoded in the residual interaction among the Fermi-liquid quasiparticles $V(\mathbf{q})$, after renormalizing the Fermi Liquid via the slave boson approach. At and above optimum doping, the transition is ruled by quantum and thermal CDW fluctuations, whereas at low doping phase fluctuations control the reduction of the stiffness and determine the transition. Our main result is that only one *bona fide* dome-shaped CDW transition line is present, ending into two CDW-QCPs. The low doping one at $p'_c \approx 0.08$ marks the onset of a static CDW order as revealed by Fermi surface reconstruction with electron pockets. The CDW phase ends at higher doping $p_c \approx 0.16$, above which fluctuations destroy again the static order. The whole region below our mean-field line (theoretically related to T^* since it tracks its behavior) is characterized by increasingly stronger fluctuations for doping $p_c < p < p^* \approx 0.19$. Nonetheless, depending on the probe characteristic time scale, fast probes, like x rays,

detect different onset lines $T_{CDW}(p)$, well accounted for within our dynamical CDW fluctuation approach. Extrapolating these lines to low temperature may erroneously lead to a misplacement of the real CDW-QCPs. This unifying picture is also supported by the fact that, although different experiments mark distinct onsets for the static CDW transition (under strong magnetic fields) and for the dynamical regime detected by x rays, the same in-plane modulation vector is observed [61] denoting their common origin. The experiment on the c-axis optical conductivity on multilayer systems, suggested in Sec. IV, could further support the relevance of CDW phase fluctuations in determining the low-doping transition line.

Within our scenario the effective quasiparticle interactions are strongly anisotropic as a result of the anisotropy of CDW fluctuations mediating them. Starting below $T^*(p)$, this scattering accounts for a progressive increase of R_H as observed in Hall experiments. Although in YBCO the situation is not yet settled, this anisotropic scattering may be supported by other mechanisms (like pair fluctuations) to reconstruct the Fermi surface arcs and pockets with effective hole number eventually tending to p as it likely occurs in other cuprate families [47]. The interplay between CDW fluctuations and pairing is an old issue [37], which might also explain why under the action of increasingly stronger magnetic fields the superconducting dome splits in two smaller domes (see Fig. 4(b) in Ref. [62]), showing that superconductivity survives longer in the critical regions associated to the two QCPs at $p'_c = 0.08$ and $p_c = 0.16$. This tight relationship between superconductivity and CDW criticality as it clearly emerges from these experiments further supports CDW quantum criticality in the cuprates phase diagram.

APPENDIX A: THE MICROSCOPIC MODEL: MEAN-FIELD AND FLUCTUATION CORRECTED CDW INSTABILITY

We first obtain a mean-field phase diagram within the random-phase approximation (RPA) for correlated single-band quasiparticles. Specifically, we assume that a strong Hubbard-like local repulsion U can be treated with a standard slave-boson/Gutzwiller (SB/G) approach [38,63], leading to a Fermi-liquid scheme where the quasiparticles are effectively described by the Hamiltonian

$$H = \sum_{\mathbf{k},\sigma} E_{\mathbf{k}} c^\dagger_{\mathbf{k},\sigma} c_{\mathbf{k},\sigma} + \frac{1}{2} \sum_{\mathbf{q}} V(\mathbf{q}) \rho_{\mathbf{q}} \rho_{-\mathbf{q}},$$

where $c^\dagger_{\mathbf{k},\sigma}$ ($c_{\mathbf{k},\sigma}$) creates (annihilates) a quasiparticle with momentum $\mathbf{k}$ and spin projection σ. The band takes a tight-binding form $E_{\mathbf{k}} = -2t(\cos k_x + \cos k_y) + 4t' \cos k_x \cos k_y - \mu$ (we take a unit lattice spacing $a = 1$ on the CuO$_2$ planes of the cuprates, so that momenta

are dimensionless), with nearest (t) and next-to-nearest (t') neighbor hopping terms and μ is the chemical potential. $\rho_{\mathbf{q}} = \sum_{\mathbf{k},\sigma} c^\dagger_{\mathbf{k}+\mathbf{q},\sigma} c_{\mathbf{k},\sigma}$ is the Fourier transform of the density operator, and $V(\mathbf{q})$ is the residual density-density interaction between the quasiparticles. In particular, we find that $V(\mathbf{q}) = U(\mathbf{q}) - \lambda + V_c(\mathbf{q})$ arises from three contributions, each with a clear physical meaning:

$$U(\mathbf{q}) = U_0 + U_1(2 - \cos q_x - \cos q_y)$$
$$+ U_2(1 - \cos q_x \cos q_y)$$

is a short-range residual repulsion between the quasiparticles; λ is a generic local attraction that would drive a phase separation instability of the quasiparticles, were it not for the presence of a long-range Coulomb repulsion

$$V_c(\mathbf{q}) = \frac{v_c}{\sqrt{G_{\mathbf{q}}^2 - 1}},$$

which is the Fourier transform of the long-range Coulomb interaction, projected onto a single CuO$_2$ plane, preventing phase separation of the charged electrons. The coupling constant is $v_c = e^2 d/(2\epsilon_\perp)$, and

$$G_{\mathbf{q}} = 1 + \frac{\epsilon_\parallel d^2}{\epsilon_\perp}(2 - \cos q_x - \cos q_y).$$

Here, e is the electron charge, d is the interlayer distance (in units of the lattice spacing on the CuO$_2$ planes), $\epsilon_\parallel$ and $\epsilon_\perp$ are the components of the dielectric tensor for a system with tetragonal symmetry, along the principal axes parallel and perpendicular to the CuO$_2$ planes, respectively. For the sake of definiteness we fix for YBCO, $\epsilon_\perp = 5$, $\epsilon_\parallel = 20$. As we shall see, the Coulomb repulsion changes the electronic phase-separation instability at $\mathbf{q} = 0$ into a CDW instability at some finite vave vector $\mathbf{q} = \mathbf{q}_c$.

Within a SB/G approach, the quasiparticle dispersion is suppressed by the hole doping p, i.e., $t = t_{bare} p$ and $t' = t'_{bare} p$. For YBCO, suitable values are $t_{bare} = 0.3$ eV and $t'/t = -0.45$.

At a given doping p, the chemical potential μ is fixed by the equation

$$\frac{2}{N} \sum_{\mathbf{k}} f(E_{\mathbf{k}}) = 1 - p,$$

where N is the number of $\mathbf{k}$ vectors within the first Brillouin zone of the CuO$_2$ planes, and $f(z) = (1 + e^{z/T})^{-1}$ is the Fermi distribution function at a temperature T. The parameters of the short-range repulsion are then found as [38] $U_0 = -4\mu/p$,

$$U_1 = \frac{t_{bare}}{pN} \sum_{\mathbf{k}} (\cos k_x + \cos k_y) f(E_{\mathbf{k}})$$

and

$$U_2 = \frac{4t'_{bare}}{pN} \sum_{\mathbf{k}} \cos k_x \cos k_y \, f(E_{\mathbf{k}}).$$

The Coulomb interaction prevents the segregation of charged quasiparticles on large scales, driven by λ, while leading to a finite-wavelength instability at $\mathbf{q} = \mathbf{q}_c$. These are the basic ingredients of the so-called frustrated-phase-separation mechanism [30,31] underlying the formation of CDW near

FIG. 5. Feynman diagrams for the CDW field. (a) Four-leg vertex representing the interaction between CDW fields. (b) First-order self-energy correction to the CDW fluctuation propagator.

optimal doping [25]. We notice that, while this model has been considered in the past to describe a phonon-mediated short-range attraction, λ can well describe any short-ranged (i.e., weakly momentum dependent) attraction possibly arising from nearest-neighbor magnetic [64], Coulombic [65,66] or/and phononic [25,67] mechanisms. The intraband screening processes can be described by the standard quasiparticle Lindhard polarization bubble

$$\Pi(\mathbf{q}, \omega_n) = -\sum_{\mathbf{k},\sigma} \frac{f(E_{\mathbf{k}+\mathbf{q}}) - f(E_{\mathbf{k}})}{E_{\mathbf{k}+\mathbf{q}} - E_{\mathbf{k}} + i\omega_n}, \qquad \text{(A1)}$$

where ω_n are bosonic Masubara frequencies. Electronic charge instabilities within the RPA approximation are found by imposing a divergent density-density response, i.e., a vanishing denominator $1 + V(\mathbf{q}_c)\Pi(\mathbf{q}_c, 0) = 0$ first occurring at some finite $\mathbf{q} = \mathbf{q}_c$. To find the RPA instability line we first adjust λ and V_c to match the instability point with the doping $p = p^* \approx 0.19$ at which the pseudogap crossover line $T^*(p)$ extracted from resistivity data extrapolates for $T \to 0$. Once the parameters of $V(\mathbf{q})$ are fixed, the instability is found at finite T by considering the T dependence of the polarization bubble Eq. (A1) only. The resulting instability line is given by the magenta line in Fig. 1, remarkably fitting the entire experimental $T^*(p)$ line.

Expanding $V(\mathbf{q})$ and $\Pi(\mathbf{q}, \omega_n)$ around $\mathbf{q}_c$ and $\omega_n = 0$, one obtains the standard expression (1) for the quantum-critical charge fluctuation propagator [25,53]. The frequency cutoff $\overline{\Omega}$ is related to the characteristic energy scale of the short-range interaction mediators (e.g., for phonons of typical energy ω_0, $\overline{\Omega} \sim \omega_0^2/t \sim \omega_0/5 \sim 10$ meV [53]). Above the mean-field QCP, the mass term $m_0 \propto \xi^{-2} \sim T^2$ increases, due to reduction of the correlation length ξ.

This behavior is modified by the first perturbative correction beyond RPA. Within the standard derivation of a Ginzburg-Landau description of criticality in fermion systems [68,69], this correction comes from the $u\Psi^4$ interaction between charge fluctuation fields Ψ, which is depicted in Fig. 5(a). The mass correction comes from the contraction of two legs and is represented by the diagram in Fig. 5(b).

To obtain the blue solid line in Fig. 1 we solved Eq. (2) fixing $\Lambda = 1800$ K and $\overline{\Omega} = 130$ K according to the values obtained fitting Raman spectra in Ref. [70]. Then the coupling $u = 600$ K (corresponding to a dimensionless coupling $u/\Lambda = 1/3$) was adjusted to match the shifted QCP with the experimental value $p_c \approx 0.16$. The green line in Fig. 1 is instead obtained by setting $m = \omega_{\mathrm{pr}} = 50$ K.

APPENDIX B: HALL COEFFICIENT WITHIN THE CDW-QCP MODEL

The in-plane longitudinal and transverse conductivities have been derived in Ref. [71] and read

$$\sigma_{xx} = \frac{e^2}{\pi^3 \hbar} \frac{2\pi}{d} \int d\phi \, \frac{k_F v_F \cos^2(\phi)}{\Gamma(\phi)}, \qquad \text{(B1)}$$

$$\sigma_{xy} = \frac{e^3 H}{\pi^3 \hbar^2} \frac{2\pi}{d} \int d\phi \, \frac{v_F \cos(\phi)}{\Gamma(\phi)} \frac{\partial}{\partial \phi} \frac{v_F \sin(\phi)}{\Gamma(\phi)}, \quad \text{(B2)}$$

where $\Gamma(\phi)$ is the anisotropic scattering rate along the Fermi surface (ϕ denotes the angle between the in-plane momentum and its $x -$ direction). Following the analysis of Ref. [18], we neglect the dependence of Fermi momentum k_F and Fermi velocity v_F on ϕ and evaluate these quantities from

$$v_F = \frac{\hbar k_F}{m^*}, \quad k_F = \frac{\sqrt{2\pi(1+p)}}{a},$$

with hole doping p and an effective mass $m^* = 4.1 \, m_e$. The in-plane lattice constant for YBCO is taken as $a = 3.85$ Å and the distance between planes is $d = 3.2$ Å. The Hall coefficient and longitudinal resistivity are then

$$R_H = \frac{\sigma_{xy}}{\sigma_{xx}^2 + \sigma_{xy}^2} \frac{1}{H},$$

$$\rho_{xx} = \frac{\sigma_{xx}}{\sigma_{xx}^2 + \sigma_{xy}^2}, \qquad \text{(B3)}$$

which we calculated in the $H \to 0$ limit. As discussed in the main text our model for the anisotropic scattering rate Eq. (3) is derived from the self-energy for quasiparticles subject to quantum critical fluctuations in the spin [45] or charge [44] channel. It is limited by a maximum scattering rate $\Gamma_{\max} = v_F/a$ and impurity scattering is considered via a (doping independent) elastic scattering rate which we fix to $\Gamma_0 = 0.86$ THz. The specific form for the quantum critical scattering Eq. (4) comprises an anisotropic and doping dependent mass $M(\phi) = m_0(T) + \bar{v} \sin^2(2\phi)$ which is minimized at the hot spots for CDW scattering, i.e., around the antinodal points $\phi = 0, \pi/2$. The parameter $\bar{v} = 480$ K is an electronic energy scale [53], whereas $m_0(T)$ is obtained self-consistently by solving Eq. (2).

The dashed lines in Fig. 6 report the temperature dependent mass for four doping values, as determined from Eq. (2) in the calculations for the phase diagram reported in Fig. 1. However, since our theory is only valid in the quantum critical region we cutoff the mass at a value $m_{\max} = 255$ K, which yields the solid lines in Fig. 6. Moreover, for doping $p = 0.19$ we also cutoff the divergence at low temperature which is due to a reentrant behavior caused by the nearby van Hove singularity. We want to stress that these cutoffs do not influence on our main conclusion, which is drawn from the significant doping dependent change of R_H at $T = 50$ K, but allow us to fit R_H over a larger temperature interval as shown in Fig. 3 of the main text.

The only fit parameters for the four doping values are the overall coupling Γ_2 and the parameter α [cf. Eq. (4)], which governs the anisotropy of the coupling to the quantum critical CDW fluctuations. The doping dependence of these parameters is shown in the inset to Fig. 7. The anisotropy parameter α strongly increases upon approaching the QCP and determines
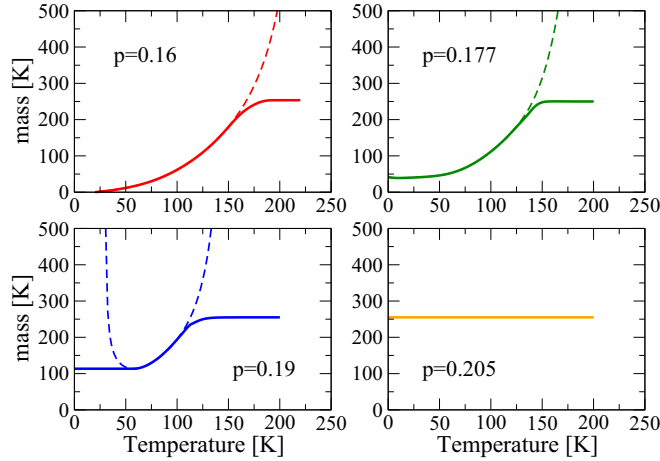
FIG. 6. Dashed lines: temperature dependence of the mass term $m_0(T)$ as determined from Eq. (2) for the four doping values considered in the paper. Solid lines include a cutoff $m_{\max} = 255$ K and $m_{\min} = 112$ K (for $p = 0.19$).

the total coupling as shown in the inset to Fig. 3 in the main text. For the same parameter values Fig. 7 reports the temperature dependence of the longitudinal conductivity as compared to the high-field normal state data from Ref. [18]. Despite an offset between the data and the results of our calculation (not surprising due to the simplicity of our model), we find an improved agreement in comparison to the calculations carried out in Ref. [18] [see their Fig. 9(d)], which was based on a scattering model which anisotropy increases linearly in temperature whereas at higher temperature a Fermi liquid type T^2 contribution dominates. In our model, the low-temperature regime is usually Fermi liquid like (except at the QCP), whereas the linear temperature regime is intermediate before crossing over to a $\sqrt{T}$-like behavior. Even more importantly, the anisotropic scattering model adopted in Ref. [18] did not consider the critical temperature and doping dependence of the mass of the scattering mediator obtained by us via
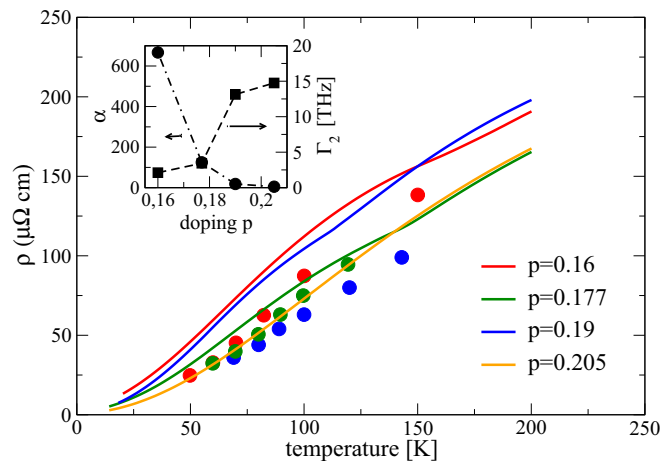
FIG. 7. Fits of the longitudinal resistivity Eq. (B3) as compared to the high-field normal state data (full dots) from Ref. [18]. (Inset) Doping dependence of the fit parameters α (solid circles) and Γ_2 (solid squares).

an independent analysis (see Fig. 6). This improvement, leading to a spread in temperature between the calculated ρ's substantially lower than in Fig. 9(d) of Ref. [18], indicates that criticality is a crucial ingredient in this region of the phase diagram and that the anisotropic scattering model cannot be ruled out as simply as it is claimed there.

As discussed in the main text, we disregard here the additional effect of pair fluctuations. While this will likely reduce the request of strong anisotropic CDW-mediated scattering (the parameter α) it naturally reduces the value of resistivity improving the agreement between calculated and experimental resistivity).

APPENDIX C: CDW SUPPRESSION BY PHASE FLUCTUATIONS

We started from a bare CDW phase stiffness $D_0 = A\,p$ linearly increasing with doping as a result of strong correlations near the Mott-Hubbard transition. In the absence of experimental indications on the value of A, we took $A = 5800$ K, which fixes $D_0 = 580$ K at $p = 0.1$. This choice is rather immaterial in the forthcoming discussion, where we highlight the dependence of the outcomes of our calculations on quantities that can be accessed by experiments. Of course, any experimental determination of D_0 is accommodated by a change of the other model parameters, so as to keep fixed the measurable quantities.

The reduction of the stiffness in Eq. (5) can be cast in a more convenient way by using the semiclassical approximation for the Bose function $b(z) \approx T/z$ yielding

$$D(T) = D_0\left[1 - \frac{u_\theta c_\theta \Lambda_\theta}{6\pi D_0}\left(1 + \frac{3T}{2c_\theta \Lambda_\theta}\right)\right].$$

The BKT transition is obtained when $D = 2T/\pi$. We point out that, even if this transition were not ruled by the two-dimensional BKT physics, Eq. (5) nonetheless implies a transition at a temperature T_θ, where the D vanishes (see blue dotted line in the inset of Fig. 4). T_θ is obviously higher than T_{BKT}, where D is still finite.

We define the dimensionless quantity $\widetilde{T} = 3T/(2c_\theta \Lambda_\theta)$ and the dimensionless bare BKT temperature $\widetilde{T}_0 = 3T_0/(2c_\theta \Lambda_\theta)$, using the characteristic energy scale of the phase mode $c_\theta \Lambda_\theta$ as an energy unit. Taking for the sake of convenience $\tilde{u} = u_\theta/8$, we obtain from the above equation the condition for the BKT transition temperature suppressed by phase fluctuations, $\widetilde{T} = \widetilde{T}_0 - \tilde{u}(1 + \widetilde{T})$. Within this approximation, the critical BKT line is then

$$\widetilde{T} = \frac{\widetilde{T}_0 - \tilde{u}}{1 + \tilde{u}},$$

while from the definition of $\widetilde{T}_0$ and c_θ, we find $\widetilde{T}_0 = \beta\sqrt{p}$ with $\beta = 3\sqrt{A\chi}/(2\Lambda_\theta)$. The condition for a QCP where the BKT transition temperature vanishes is then given by $\widetilde{T}_0 = \tilde{u}$, which also defines the critical doping $p_c' \approx 0.08$ fixed by experiments [18]. Expanding around this value, we find the equation for the critical line

$$\widetilde{T} = \frac{\tilde{u}}{2(1 + \tilde{u})\sqrt{p_c'}}(p - p_c').$$

The slope of the physical $T_{CDW}(p)$ line is obtained by reintroducing the characteristic energy scale $c_\theta \Lambda_\theta$,

$$\frac{c_\theta \Lambda_\theta \tilde{u}}{2(1 + \tilde{u})\sqrt{p'_c}},$$

and is fixed by fitting the data (light-blue squares in Fig. 1). In this way, the various physically relevant combinations of the microscopic parameters have been reduced to two effective parameters only, the position of the QCP and the slope of the $T_{CDW}(p)$ curve, which can be fixed by experiments. Specifically, we obtain the dashed blue line in Fig. 1 with $\tilde{u} = 4.5$, and the characteristic energy scale $c_\theta = 850\sqrt{p}$ K and numerically solving the full expression Eq. (5).

APPENDIX D: INFLUENCE OF CDW SCATTERING ON THE FERMI SURFACE QUASIPARTICLE WEIGHT

The hamiltonian of an electronic system subject to CDW scattering is given by

$$H = \sum_{k,\sigma} \varepsilon_k c^\dagger_{k,\sigma} c_{k,\sigma} + \sum_{k,q,\sigma} g(q) c^\dagger_{k+q,\sigma} c_{k,\sigma}, \qquad \text{(D1)}$$

where $g(q) = 1/N \sum_n e^{iqR_n} V(R_n)$ is the Fourier transform of a local charge modulation potential $V(R_n)$.

We assume $g(q)$ to be enhanced at the four equivalent wave vectors $(\pm Q_{CDW}, 0)$ and $(0, \pm Q_{CDW})$:

$$g(q) = g_0 \sum_{i=1,4} \frac{\Gamma}{\Gamma^2 + \alpha^i_q}, \qquad \text{(D2)}$$

where Γ corresponds to the inverse of the CDW correlation length and $\alpha^{1,2}_q = 2 - \cos(q_x \pm Q_{CDW}) - \cos(q_y)$, $\alpha^{3,4}_q = 2 - \cos(q_x) - \cos(q_y \pm Q_{CDW})$. Figure 8 shows the function $g(q)$ for $\Gamma = 0.3[1/a]$ and $Q_{CDW} = 2\pi/6[1/a]$ similar to the parameters used in Ref. [38]. Upon diagonalizing the Hamiltonian Eq. (D1) one obtains the Fermi surface reported in panel (b) of Fig. 8. Clearly the CDW scattering reduces strongly the spectral weight around the antinodal regions,
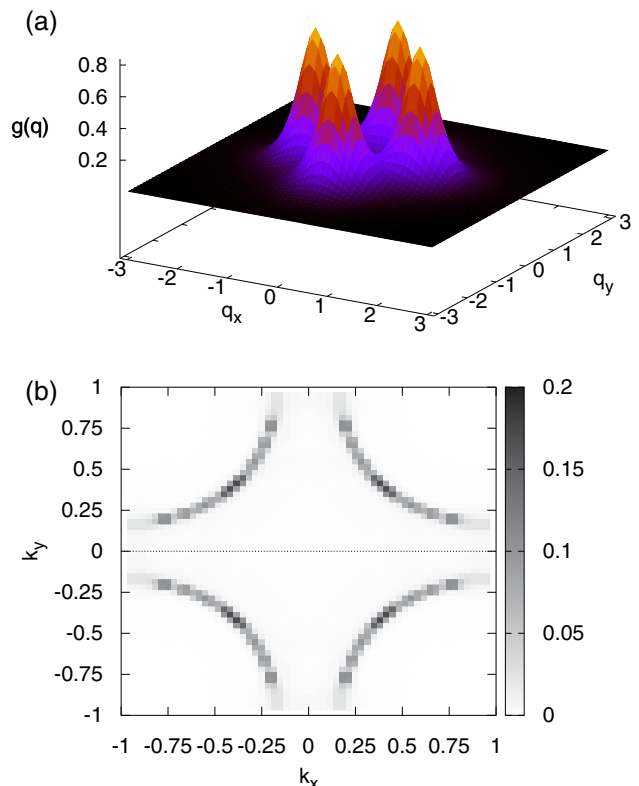
FIG. 8. (a) The function $g(q)$ of Eq. (D2), which describes the momentum structure of CDW scattering. (b) The resulting Fermi surface for doping $n = 0.15$.

while any shadow features produced by the CDW scattering are well below the scale of visibility. This is all we need to identify the onset of CDW fluctuations T_{CDW^0} with the pseudogap crossover temperature T^*. At lower temperature, the situation is much more involved and one might speculate that CDW interplay with pairing (see, e.g., Ref. [40]) leading to the formation of Fermi arcs.

[1] G. Ghiringhelli, M. Le Tacon, M. Minola, S. Blanco-Canosa, C. Mazzoli, N. B. Brookes, G. M. De Luca, A. Frano, D. G. Hawthorn, F. He, T. Loew, M. Moretti Sala, D. C. Peets, M. Salluzzo, E. Schierle, R. Sutarto, G. A. Sawatzky, E. Weschke, B. Keimer, and L. Braicovich, Long-range incommensurate charge fluctuations in (Y, Nd)Ba$_2$Cu$_3$O$_{6+x}$, Science **337**, 821 (2012).

[2] J. Chang, E. Blackburn, A. T. Holmes, N. B. Christensen, J. Larsen, J. Mesot, R. Liang, D. A. Bonn, W. N. Hardy, A. Watenphul, M. V. Zimmermann, E. M. Forgan, and S. M. Hayden, Direct observation of competition between superconductivity and charge density wave order in YBa$_2$Cu$_3$O$_{6.67}$, Nat. Phys. **8**, 871 (2012).

[3] R. Comin, A. Frano, M. M. Yee, Y. Yoshida, H. Eisaki, E. Schierle, E. Weschke, R. Sutarto, F. He, A. Soumyanarayanan, Yang He, M. Le Tacon, I. S. Elfimov, J. E. Hoffman, G. A. Sawatzky, B. Keimer, and A. Damascelli, Charge order driven

by fermi-arc instability in Bi$_2$Sr$_{2-x}$La$_x$CuO$_{6+d}$, Science **343**, 390 (2014).

[4] S. Blanco-Canosa, A. Frano, E. Schierle, J. Porras, T. Loew, M. Minola, M. Bluschke, E. Weschke, B. Keimer, and M. Le Tacon, Resonant X-ray scattering study of charge-density-wave correlations in YBa$_2$Cu$_3$O$_{6+x}$, Phys. Rev. B **90**, 054513 (2014).

[5] T. Wu, H. Mayaffre, S. Krämer, M. Horvatić, C. Berthier, W. N. Hardy, R. Liang, D. A. Bonn, and M.-H. Julien, Magnetic-field-induced charge-stripe order in the high-temperature superconductor YBa$_2$Cu$_3$O$_y$, Nature (London) **477**, 191 (2011).

[6] T. Wu, H. Mayaffre, S. Krämer, M. Horvatić, C. Berthier, P. L. Kuhns, A. P. Reyes, R. Liang, W. N. Hardy, D. A. Bonn, and M.-H. Julien, Emergence of charge order from the vortex state of a high-temperature superconductor, Nat. Commun. **4**, 2113 (2013).

[7] P. W. Anderson *The Theory of Superconductivity in the High-T_c Cuprate Superconductors* (Princeton University Press, 1997).

[8] N. Nagaosa and P. A. Lee, Normal-State Properties of the Uniform Resonating-Valence-Bond State, Phys. Rev. Lett. **64**, 2450 (1990); P. A. Lee and N. Nagaosa, Gauge theory of the normal state of high-T_c superconductors, Phys. Rev. B **46**, 5621 (1992).

[9] K.-Y. Yang, T. M. Rice, and F.-C. Zhang, Phenomenological theory of the pseudogap state, Phys. Rev. B **73**, 174501 (2006); T. M. Rice, K.-Y. Yang, and F. C. Zhang, A phenomenological theory of the anomalous pseudogap phase in underdoped cuprates, Rep. Prog. Phys. **75**, 016502 (2012).

[10] For a recent overview see, e.g., S. Sachdev, Emergent gauge fields and the high temperature superconductors, Philos. Trans. R. Soc. A **374**, 20150248 (2016).

[11] C. Castellani, C. Di Castro, and W. Metzner, Dimensional Crossover from Fermi to Luttinger Liquid, Phys. Rev. Lett. **72**, 316 (1994).

[12] C. Castellani, C. Di Castro, and M. Grilli, Non-Fermi-liquid behavior and d-wave superconductivity near the charge-density-wave quantum critical point, Z. Phys. B **103**, 137 (1996).

[13] C. Castellani, C. Di Castro, and M. Grilli, Stripe formation: A quantum critical point for cuprate superconductors, J. Phys. Chem. Solids **59**, 1694 (1998).

[14] S. A. Kivelson, I. P. Bindloss, E. Fradkin, V. Oganesyan, J. M. Tranquada, A. Kapitulnik, and C. Howald, How to detect fluctuating stripes in the high-temperature superconductors, Rev. Mod. Phys. **75**, 1201 (2003), and references therein.

[15] D. LeBoeuf, S. Krämer, W. N. Hardy, R. Liang, D. A. Bonn, and C. Proust, Thermodynamic phase diagram of static charge order in underdoped YBa$_2$Cu$_3$O$_y$, Nat. Phys. **9**, 79 (2013).

[16] N. Doiron-Leyraud, C. Proust, D. LeBoeuf, J. Levallois, J.-B. Bonnemaison, R. Liang, D. A. Bonn, W. N. Hardy, and L. Taillefer, Quantum oscillations and the Fermi surface in an underdoped high-T_c superconductor, Nature (London) **447**, 565 (2007).

[17] S. E. Sebastian, N. Harrison, G. G. Lonzarich, Towards resolution of the Fermi surface in underdoped high-T_c superconductors, Rep. Prog. Phys. **75**, 102501 (2012).

[18] S. Badoux, W. Tabis, F. Laliberté, G. Grissonnanche, B. Vignolle, D. Vignolles, J. Béard, D. A. Bonn, W. N. Hardy, R. Liang, N. Doiron-Leyraud, L. Taillefer, and C. Proust, Change of carrier density at the pseudogap critical point of a cuprate superconductor, Nature (London) **531**, 210 (2016).

[19] T. Wu, H. Mayaffre, S. Krämer, M. Horvatić, C. Berthier, W. N. Hardy, R. Liang, D. A. Bonn, and M.-H. Julien, Incipient charge order observed by NMR in the normal state of YBa$_2$Cu$_3$O$_y$, Nat. Commun. **6**, 6438 (2015).

[20] E. H. da Silva Neto, P. Aynajian, A. Frano, R. Comin, E. Schierle, E. Weschke, A. Gyenis, J. Wen, J. Schneeloch, Z. Xu, S. Ono, G. Gu, M. Le Tacon, and A. Yazdani, Ubiquitous interplay between charge ordering and high-temperature superconductivity in cuprates, Science **343**, 393 (2014).

[21] M. H. Hamidian, S. D. Edkins, C. K. Kim, J. C. Séamus Davis, A. P. Mackenzie, H. Eisaki, S. Uchida, M. J. Lawler, E.-A. Kim, S. Sachdev, and K. Fujita, Atomic-scale electronic structure of the cuprate d-symmetry form factor density wave state, Nat. Phys. **12**, 150 (2016).

[22] M. Hücker, N. B. Christensen, A. T. Holmes, E. Blackburn, E. M. Forgan, R. Liang, D. A. Bonn, W. N. Hardy, O. Gutowski, M. v. Zimmermann, S. M. Hayden, and J. Chang, Competing charge, spin, and superconducting orders in underdoped YBa$_2$Cu$_3$O$_y$, Phys. Rev. B **90**, 054514 (2014).

[23] Y. Ando, S. Komiya, K. Segawa, S. Ono, and Y. Kurita, Electronic Phase Diagram of High-T_c Cuprate Superconductors from a Mapping of the In-Plane Resistivity Curvature, Phys. Rev. Lett. **93**, 267001 (2004).

[24] O. Cyr-Choinière, G. Grissonnanche, S. Badoux, J. Day, D. A. Bonn, D. N. Hardy, R. Liang, N. Doiron-Leyraud, and L. Taillefer, Two types of nematicity in the phase diagram of the cuprate superconductor YBa$_2$Cu$_3$O$_y$, Phys. Rev. B **92**, 224502 (2015).

[25] C. Castellani, C. Di Castro, and M. Grilli, Singular Quasiparticle Scattering in the Proximity of Charge Instabilities, Phys. Rev. Lett. **75**, 4650 (1995).

[26] S. Andergassen, S. Caprara, C. Di Castro, and M. Grilli, Anomalous Isotopic Effect Near the Charge-Ordering Quantum Criticality, Phys. Rev. Lett. **87**, 056401 (2001).

[27] S. Badoux, S. A. A. Afshar, B. Michon, A. Ouellet, S. Fortier, D. LeBoeuf, T. P. Croft, C. Lester, S. M. Hayden, H. Takagi, K. Yamada, D. Graf, N. Doiron-Leyraud, and L. Taillefer, Critical Doping for the Onset of Fermi-Surface Reconstruction by Charge-Density-Wave Order in the Cuprate Superconductor La$_{2-x}$Sr$_x$CuO$_4$, Phys. Rev. X **6**, 021004 (2016).

[28] G. Seibold, M. Capati, C. Di Castro, M. Grilli, and J. Lorenzana, Hidden ferronematic order in underdoped cuprates, Phys. Rev. B **87**, 035138 (2013).

[29] M. Capati, S. Caprara, C. Di Castro, M. Grilli, G. Seibold, and J. Lorenzana, Electronic polymers and soft-matter-like broken symmetries in underdoped cuprates, Nat. Commun. **6**, 7691 (2015).

[30] R. Raimondi, C. Castellani, M. Grilli, Y. Bang, and G. Kotliar, Charge collective modes and dynamic pairing in the three band Hubbard model: Strong coupling limit, II, Phys. Rev. B **47**, 3331 (1993).

[31] V. J. Emery and S. A. Kivelson, Frustrated electronic phase separation and high-temperature superconductors, Physica C **209**, 597 (1993).

[32] V. J. Emery, S. A. Kivelson, and H. Q. Lin, Phase Separation in the *T-J* Model., Phys. Rev. Lett. **64**, 475 (1990).

[33] M. Tsuchiizu, Y. Yamakawa, and H. Kontani, p-orbital density wave with d symmetry in high-T_c cuprate superconductors predicted by renormalization-group + constrained RPA theory, Phys. Rev. B **93**, 155148 (2016).

[34] M. A. Metlitski and S. Sachdev, Quantum phase transitions of metals in two spatial dimensions. II. Spin density wave order, Phys. Rev. B **82**, 075128 (2010).

[35] K. B. Efetov, H. Meier, and C. Pepin, Pseudogap state near a quantum critical point, Nat. Phys. **9**, 442 (2013).

[36] Y. Wang and A. Chubukov, Interplay between unidirectional and bidirectional charge-density-wave orders in underdoped cuprates, Phys. Rev. B **92**, 245140 (2015).

[37] A. Perali, C. Castellani, C. Di Castro, and M. Grilli, d-wave superconductivity near charge instabilities, Phys. Rev. B **54**, 16216 (1996).

[38] G. Seibold, F. Becca, F. Bucci, C. Castellani, C. Di Castro, and M. Grilli, Spectral properties of incommensurate charge-density wave systems, Eur. Phys. J. B **13**, 87 (2000).

[39] A. Kaminski, T. Kondo, T. Takeuchi, and G. Gu, Pairing, pseudogap and Fermi arcs in cuprates, Philos. Mag. **95**, 453 (2015).

[40] A. Allais, D. Chowdhury, and S. Sachdev, Connecting high-field quantum oscillations to zero-field electron spectral functions in the underdoped cuprates, Nat. Commun. **5**, 5771 (2014).

[41] J. G. Storey, Hall effect and Fermi surface reconstruction via electron pockets in the high-T_c cuprates, Europhys. Lett. **113**, 27003 (2016).

[42] S. Sachdev, E. Berg, S. Chatterjee, and Y. Schattner, Spin density wave order, topological order, and Fermi surface reconstruction, Phys. Rev. B **94**, 115147 (2016), and references therein.

[43] A. Eberlein, W. Metzner, S. Sachdev, and H. Yamase, Fermi Surface Reconstruction and Drop of Hall Number Due to Spiral Antiferromagnetism in High-T_c Cuprates, Phys. Rev. Lett. **117**, 187001 (2016).

[44] S. Caprara, M. Sulpizi, A. Bianconi, C. Di Castro, and M. Grilli, Single-particle properties of a model for coexisting charge and spin quasi-critical fluctuations coupled to electrons, Phys. Rev. B **59**, 14980 (1999).

[45] Ar. Abanov, A. Chubukov, and J. Schmalian, Quantum-critical theory of the spin-fermion model and its application to cuprates: normal state analysis, Adv. Phys. **52**, 119 (2003), and references therein.

[46] B. J. Ramshaw, S. E. Sebastian, R. D. McDonald, J. Day, B. S. Tan, Z. Zhu, J. B. Betts, R. Liang, D. A. Bonn, W. N. Hardy, N. Harrison, Quasiparticle mass enhancement approaching optimal doping in a high-T_c superconductor, Science **348**, 317 (2015).

[47] C. Collignon, S. Badoux, A. A. Afshar, B. Michon, F. Laliberté, O. Cyr-Choinière, J.-S. Zhou, S. Licciardello, S. Wiedmann, N. Doiron-Leyraud, and L. Taillefer, Fermi-surface transformation across the pseudogap critical point of the cuprate superconductor La$_{1.6-x}$Nd$_{0.4}$Sr$_x$CuO$_4$, arXiv:1607.05693.

[48] S. E. Sebastian, N. Harrison, M. M. Altarawneh, C. H. Mielke, R. Liang, D. A. Bonn, W. N. Hardy, and G. G. Lonzarich, Metal-insulator quantum critical point beneath the high T_c superconducting dome, Proc. Natl. Acad. Sci. USA **107**, 6175 (2010).

[49] G. Grüner, The dynamics of charge-density waves, Rev. Mod. Phys. **60**, 1129 (1988).

[50] L. Nie, G. Tarjus, and S. A. Kivelson, Quenched disorder and vestigial nematicity in the pseudogap regime of the cuprates, Proc. Natl. Acad. Sci. USA **111**, 7980 (2015).

[51] L. Benfatto, A. Toschi, S. Caprara, Low-energy phase-only action in a superconductor: A comparison with the XY model, Phys. Rev. B **69**, 184510 (2004).

[52] P. A. Lee, T. M. Rice, and P. W. Anderson, Conductivity from charge or spin density waves, Solid State Commun. **14**, 703 (1974).

[53] S. Caprara, M. Grilli, C. Di Castro, and T. Enss, Optical conductivity near finite-wavelength quantum criticality, Phys. Rev. B **75**, 140505(R) (2007).

[54] A. Dubroka, M. Rössle, K. W. Kim, V. K. Malik, D. Munzar, D. N. Basov, A. A. Schafgans, S. J. Moon, C. T. Lin, D. Haug, V. Hinkov, B. Keimer, Th. Wolf, J. G. Storey, J. L. Tallon, and C. Bernhard, Evidence of a Precursor Superconducting Phase at Temperatures as High as 180 K in RBa$_2$Cu$_3$O$_{7-\delta}$(R=Y, Gd, Eu) Superconducting Crystals from Infrared Spectroscopy, Phys. Rev. Lett. **106**, 047006 (2011).

[55] D. van der Marel, and A. Tsvetkov, Transverse optical plasmons in layered superconductors, Czech. J. Phys. **46**, 3165 (1996); D. Munzar, C. Bernhard, A. Golnik, J. Humlíĉek, and M. Cardona, Anomalies of the infrared-active phonons in under-doped YBa$_2$Cu$_3$O$_y$ as evidence for the intrabilayer Josephson effect, Solid State Commun. **112**, 365 (1999); M. Grüninger, D. van der Marel, A. A. Tsvetkov, and A. Erb, Observation of Out-of-Phase Bilayer Plasmons in YBa$_2$Cu$_3$O$_{7-\delta}$, Phys. Rev. Lett. **84**, 1575 (2000).

[56] S. Caprara, C. Di Castro, M. Grilli, and G. Seibold (unpublished).

[57] P. A. Volkov and K. B. Efetov, Spin-fermion model with overlapping hot spots and charge modulation in cuprates, Phys. Rev. B **93**, 085131 (2016).

[58] R. Comin, R. Sutarto, F. He, E. H. da Silva Neto, L. Chauviere, A. Fraño, R. Liang, W. N. Hardy, D. A. Bonn, Y. Yoshida, H. Eisaki, A. J. Achkar, D. G. Hawthorn, B. Keimer, G. A. Sawatzky, and A. Damascelli, Symmetry of charge order in cuprates, Nat. Mater. **14**, 796 (2015).

[59] K. Fujita, M. H. Hamidian, S. D. Edkins, Chung Koo Kim, Y. Kohsaka, M. Azuma, M. Takano, H. Takagi, H. Eisaki, S. Uchida, A. Allais, M. J. Lawler, E.-A. Kim, Subir Sachdev, J. C. S. Davis, Direct phase-sensitive identification of a d-form factor density wave in underdoped cuprates, Proc. Natl. Acad. Sci. USA **111**, E3026 (2014).

[60] M. Vojta, Lattice symmetry breaking in cuprate superconductors: stripes, nematics, and superconductivity, Adv. Phys. **58**, 699 (2009).

[61] S. Gerber, H. Jang, H. Nojiri, S. Matsuzawa, H. Yasumura, D. A. Bonn, R. Liang, W. N. Hardy, Z. Islam, A. Mehta, S. Song, M. Sikorski, D. Stefanescu, Y. Feng, S. A. Kivelson, T. P. Devereaux, Z.-X. Shen, C.-C. Kao, W.-S. Lee, D. Zhu, J.-S. Lee, Three-dimensional charge density wave order in YBa$_2$Cu$_3$O$_{6.67}$ at high magnetic fields, Science **350**, 949 (2015).

[62] G. Grissonnanche, O. Cyr-Choinière, F. Laliberté, S. R. de Cotret, A. Juneau-Fecteau, S. Dufour-Beauséjour, M.-E. Delage, D. LeBoeuf, J. Chang, B. J. Ramshaw, D. A. Bonn, W. N. Hardy, R. Liang, S. Adachi, N. E. Hussey, B. Vignolle, C. Proust, M. Sutherland, S. Krämer, J.-H. Park, D. Graf, N. Doiron-Leyraud, and Louis Taillefer, Direct measurement of the upper critical field in cuprate superconductors, Nat. Commun. **5**, 3280 (2014).

[63] E. Arrigoni, C. Castellani, M. Grilli, R. Raimondi, and G. C. Strinati, Functional integral formulation of the slave-boson approach: beyond the mean-field treatment with the correct continuum limit, Phys. Rep. **241**, 291 (1994).

[64] C. Castellani, M. Grilli, and G. Kotliar, Mean field phase diagram of a two band t-J model for CuO$_2$ Layers., Phys. Rev. B **43**, 8000 (1991).

[65] M. Grilli, R. Raimondi, C. Castellani, C. Di Castro, and G. Kotliar, Superconductivity, Phase Separation and Charge Transfer Instability in the $U = \infty$ Limit of the Three Band Model of the CuO$_2$ Planes, Phys. Rev. Lett. **67**, 259 (1991).

[66] F. Becca, F. Bucci, and M. Grilli, Incommensurate charge-density-wave instability in the extended three-band Hubbard model, Phys. Rev. B **57**, 4382 (1998).

[67] F. Becca, M. Tarquini, M. Grilli, and C. Di Castro, Charge-Density-Waves and superconductivity as an alternative to phase separation in the infinite-U Hubbard-Holstein model, Phys. Rev. B **54**, 12443 (1996).

[68] J. A. Hertz, Quantum critical phenomena, Phys. Rev. B **14**, 1165 (1976).

[69] A. J. Millis, Effect of a nonzero temperature on quantum critical points in itinerant fermion systems, Phys. Rev. B **48**, 7183 (1993).

[70] S. Caprara, C. Di Castro, B. Muschler, W. Prestel, R. Hackl, M. Lambacher, A. Erb, S. Komiya, Y. Ando, and M. Grilli, Extracting the dynamical effective interaction and competing order from an analysis of Raman spectra of the high-temperature La$_{2-x}$Sr$_x$CuO$_4$ superconductor, Phys. Rev. B **84**, 054508 (2011).

[71] N. E. Hussey, The normal state scattering rate in high-T_c cuprates, Eur. Phys. J. B **31**, 495 (2003).